A Mechanistic Model of Top-of-the-Line Corrosion

Z. Zhang,[‡,] D. Hinkson,[*] M. Singer,[*] H. Wang,[*] and S. Nešić[*]*

ABSTRACT

A mechanistic model is developed to predict the general corrosion rate at the top of a gas pipeline. This model covers the three main processes involved in the top-of-the-line corrosion (TLC) phenomena: the dropwise condensation, the behavior of the chemistry in the condensed water, and the corrosion at the steel surface. The dropwise condensation process is modeled based on the heat and mass-transfer theory and is used to predict the condensation rate. The breakdown of species concentrations in the droplet is established through the main thermodynamic and chemical equilibrium. The general corrosion rate is predicted using the kinetics of the electrochemical reactions at the steel surface and by taking into account the mass-transfer and chemical reactions occurring inside the droplet. Finally, the accuracy of the predictions of the model is evaluated by comparison with experimental data.

KEY WORDS: carbon dioxide, dropwise condensation, mechanistic model, top-of-the-line corrosion

INTRODUCTION

Top-of-the-line corrosion (TLC) is a phenomenon encountered in the oil and gas industry when problems of corrosion appear inside the pipe due to the condensation of water containing dissolved corrosive gases. TLC occurs exclusively in wet gas transportation and in a stratified flow regime. Condensation happens when the environment outside the pipeline is cooler than the saturated vapor flowing inside the pipe. The water vapor in the gas phase condenses on the pipe wall in two different ways:

—on the side walls of the pipe where the condensed liquid slides to the bottom of the line due to gravity forces

—at the top of the pipe where droplets of liquid form and remain attached at the metal surface for a longer time

The dissolution of corrosive gases, such as carbon dioxide (CO_2) and hydrogen sulfide (H_2S), as well as condensation of acidic vapors such as acetic acid (HAc) in the droplet, can cause serious corrosion problems at the metal surface. The top of the line is the most critical location because severe problems of localized corrosion can occur there. The injection of chemical inhibitors (a standard method to fight corrosion issues at the bottom of the line) is not effective since they cannot reach the top of the line easily. TLC has become a growing concern in the oil and gas industry and a better understanding of the corrosion mechanisms involved is needed. Due to the limitation of previously published models,[1-6] which are either empirical or semi-empirical, a mechanistic model presented below is devised in the present study to satisfy this need.

Since Estavoyer[1] reported a case of TLC in an oil field, much work has been done in this area. Olsen and Dugstad[2] conducted a study to look at some of the key parameters in TLC. In their study the effects of temperature and condensation rate on the formation of protective iron carbonate ($FeCO_3$) scale were investigated. Also, an increase in gas flow rate was

Submitted for publication November 2006; in revised form, July 2007.

‡ Corresponding author. E-mail: zz135104@ohio.edu.

* Ohio University, Institute for Corrosion and Multiphase Technology, 342 West State St., Athens, OH 45701.

0010-9312/07/000193/$5.00+$0.50/0

found to increase the condensation rate, which, in turn, influences the corrosion at the top of the line. However, Olsen and Dugstad did not propose a model or any correlation between corrosion and the parameters they studied. In 1993, de Waard and Lotz[3] modified their corrosion model for the full pipe flow after introducing a correction factor to predict the corrosion rate at the top of the line for condensation rates below a typical field value of 0.25 mL/m^2/s. From a TLC failure in the field, Gunaltun and coworkers[4-5] gave a complete description of the TLC phenomena for the first time, forming a solid basis for future experimentation and modeling efforts. Pots and Hendriksen[6] proposed an iron supersaturation model to calculate the corrosion rate using the condensation rate and the precipitation rate of $FeCO_3$ as the two key concepts. However, without being able to reliably predict the condensation rate and regimes, and by ignoring some other important parameters, which are discussed below, this corrosion model can only be seen as a first attempt to predict TLC. Vitse, et al.,[7-8] proposed a quasi-mechanistic model to predict the corrosion rate in TLC; however, their efforts could be useful at best in describing corrosion during the filmwise condensation process, which is not common for the top of the line.

For better modeling of TLC, it is necessary to have an accurate prediction of the condensation rate and the condensation regime. In the previous work, many researchers tried to predict the condensation rate by using the filmwise condensation theory. However, large discrepancies arise when this theory is used to predict the condensation rate for the dropwise condensation process. In addition, it is essential to be able to predict the water composition in the droplets as well as any $FeCO_3$ scale formation with time.

In this work, a mechanistic condensation model will be established based on the dropwise condensation theory. This condensation model will predict droplet growth rate, which is a function of time. The chemistry inside the droplet is determined from the thermodynamic equilibrium at the liquid/gas interface and the electrochemical reactions at metal surface linked to the corrosion process. The mechanistic corrosion model presented by Nešić and coworkers[9-11] is used as a basis for all calculations and is combined with the dropwise condensation model to predict TLC phenomena. Finally, this model is verified through comparison between experimental data and predicted results.

CONDENSATION MODEL

When the condensed liquid cannot wet the wall surface completely, a discontinuous film of liquid can form on the metal surface. The dropwise condensation process at the top of the line in wet gas conditions is one type of heterogeneous condensation, in which liquid embryos first nucleate at the interface between a metastable saturated vapor and another solid phase. The size of the droplet will increase as the vapor continuously condenses on the gas-liquid interface. Coalescence happens when adjacent droplets contact each other due to the continuous increase in droplet size. Therefore, the size of the water droplet would increase by means of either direct condensation of vapor or coalescence among adjacent droplets. As the droplet size increases at high gas velocity, the droplet might start to move along in the gas flow direction as a result of drag forces from the motion of the surrounding gas, continuously sweeping other droplets on its way ahead. On the other hand, when a single droplet reaches its maximum size, it may flow down along the inner surface of the pipe wall as a result of gravity pull. In most situations a combined movement (forward and down) is seen. At very low gas velocity and very large pipe diameters, the droplets may detach from the top pipe surface and fall to the bottom. New liquid embryos will form on the locations where the old droplets were removed and the cycle of nucleation, growth, moving/falling will repeat. In many instances when droplets are removed from the surface, some water remains attached, making the nucleation less important.

In the reported field cases,[4-5] the morphology of the corroded steel surface at the top of the line indicates that dropwise condensation is more likely than the filmwise condensation. Our own experimentation including in situ visual observation and coupon analysis (Figure 1) showed clear evidence of dropwise condensation. Finally, it is known that the transition from dropwise condensation to filmwise condensation occurs at much higher heat fluxes than are typical for TLC.[12] Factors that will influence the condensation rate in the wet gas pipeline include:

—gas temperature
—subcooling temperature (defined as $\Delta T = T_b^g - T_i^w$, where T_b^g is bulk gas temperature and T_i^w is inner wall temperature)
—noncondensable gas concentration
—gas velocity
—system pressure
—internal pipe diameter

Since liquid nucleation of embryos in dropwise condensation is a random process, a statistical method (droplet size distribution function) is used to model the overall heat-transfer process. To calculate the condensation rate for dropwise condensation, two crucial parameters must first be obtained: droplet size distribution and heat-transfer rate through each droplet of a given radius, r.

Droplet-Size Distribution Function

At any given time, a family of droplets with different diameters occupies the pipe inner surface. This is called the droplet-size distribution in dropwise con-

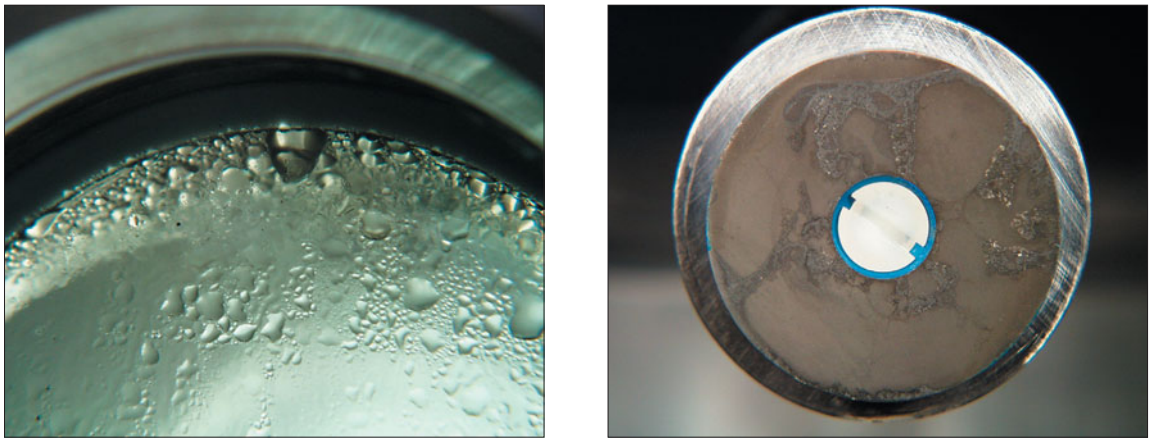

(a) (b)

FIGURE 1. *Evidence of dropwise condensation at the top of the line seen through a (a) side window and on an (b) exposed weight-loss coupon.*

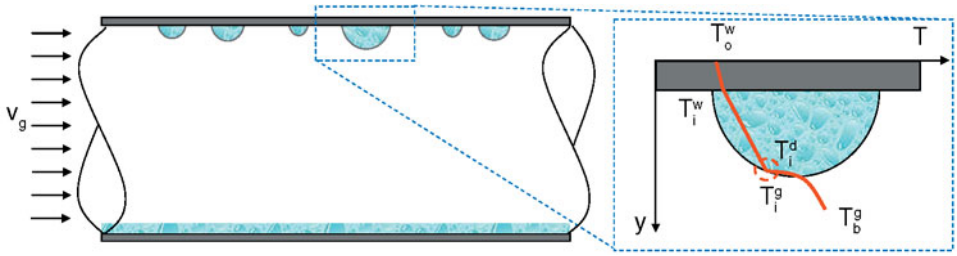

FIGURE 2. *Temperature gradient in a single droplet where the bulk temperature can be assumed to be constant for a very short distance in the flow direction. T_o^w: outer wall temperature; T_i^w: inner wall temperature; T_i^d: interfacial temperature in the liquid side; T_i^g: interfacial temperature in the gas side; T_b^g: bulk gas temperature; V_g: gas velocity.*

densation. Equation (1) was first proposed by Rose and Glicksman[13] and is one of the most commonly used droplet-size distribution functions:

$$N(r)dr = \frac{n}{\pi r^2 r_{max}}\left(\frac{r}{r_{max}}\right)^{n-1} dr \qquad (1)$$

where N(r)dr is the number of droplets at radius, r, over a 1-m^2 surface area; n is the exponent constant, typically as 1/3; and r_{max} is the maximum droplet radius, m.

Heat Flux in Dropwise Condensation

The overall heat-transfer process in dropwise condensation should take into account several crucial phenomena,[14-16] as shown in Figure 2:

—Heat-transfer resistance in the gas phase boundary layer.
—Water vapor condensation at the droplet surface.
—The influence of droplet surface curvature on the phase equilibrium temperature. This is important especially for small droplets.
—Vapor-liquid interfacial resistance. In the condensation process, only part of the vapor molecules, which are striking the liquid surface, can enter the liquid phase. This causes a thermal resistance to heat transfer.
—Heat conduction resistance through the droplets. It is important to point out that the heat conduction resistance is not uniform through a droplet, since the distance from the droplet surface (gas-liquid interface) to the inner pipe wall changes from the apex to the drop base perimeter (gas-liquid-solid three-phase interface).
—Heat conduction resistance through the pipe wall and the insulation layer to the environment.

Heat Balance

Due to the fact that the heat-transfer resistance in the gas phase is significant when noncondensable gases are present and that the phase change (vapor condensation) happens at the interface, the total flux of heat Q between the gas phase and the droplets can be written as:

$$Q = Q_g + Q_c \quad (2)$$

where Q_g is the heat flux through the gas boundary layer to the droplet surface, W/m^2, and Q_c is the latent heat flux released by the phase change at the droplet surface, W/m^2.

—For a fully developed gas boundary layer, the heat flux Q_g can be calculated by:

$$Q_g = h_g \times (T_b^g - T_i^g) \quad (3)$$

where h_g is the heat-transfer coefficient for the gas boundary layer, W/m^2/K; T_b^g is the temperature of the bulk gas, K; and T_i^g is the temperature of the gas at the droplet interface, K.

Here, the heat-transfer coefficient of the gas boundary layer in a pipeline can be estimated by empirical correlations:[17]

$$Nu = 0.023\,Re^{0.8}\,Pr^{0.4} \quad (4)$$

where $Nu = h_g d/k_g$ is the Nusselt number; $Re = v_g d\rho_g/\mu$ is the Reynolds number; $Pr = \hat{C}_p\mu/k_g$ is the Prantl number; d is the internal pipeline diameter, m; k_g is the thermal conductivity of the gas, W/m·K; v_g is the gas velocity, m/s; ρ_g is the gas density, kg/m^3, μ is the gas viscosity, Pa·s; and $\hat{C}_p$ is the heat capacity of the gas, J/K·kg.

—The latent heat flux is related to the condensation rate:

$$Q_c = \dot{m}H_{fg} \quad (5)$$

where $\dot{m}$ is the condensation rate, kg$_g$/m^2/s, and H_{fg} is the latent heat of evaporation/condensation for water, J/kg.

The total heat flux between the gas phase and the droplets becomes:

$$Q = h_g \times (T_b^g - T_i^g) + \dot{m}H_{fg} \quad (6)$$

To calculate the condensation rate $\dot{m}$ from this equation, one needs to know the heat flux Q and find the unknown temperature of the gas at the interface with the droplets T_i^g by considering that the heat transferred from the gas to the droplets passes through the droplets and the pipe wall to the outside environment.

—The temperature drop at the droplet interface due to droplet curvature is defined as:[15]

$$\Delta T_c = \frac{2T_i^g\sigma}{H_{fg}r\rho} \quad (7)$$

where r is the radius of the droplet, m; σ is the vapor-liquid surface tension, N/m; and ρ is water density, kg/m^3.

—The amount of heat q in W, carried through the interface of a droplet with a radius r, is:[15]

$$q(r) = 2\pi r^2 h_i (T_i^g - T_i^d) = 2\pi r^2 h_i \Delta T_i \quad (8)$$

where h_i is the heat-transfer coefficient at the droplet interface, W/m^2/K; T_i^d is temperature of the droplet at the interface with the gas, K; and ΔT_i is the temperature drop due to vapor-liquid interfacial resistance for a hemispherical droplet, K.

—Then, the heat is conducted through the bulk of the droplet:[16]

$$q(r) = \frac{4\pi r^2 k_{H_2O}}{r}(T_i^d - T_i^w) = 4\pi r k_{H_2O}\Delta T_d \quad (9)$$

where k_{H_2O} is the thermal conductivity of the water, W/m/K; T_i^w is temperature of the droplet at the interface with the pipe wall, K; and ΔT_d is the temperature drop due to heat conduction through a hemispherical droplet, K.

—Finally, the heat exits through the pipe wall out to the environment:

$$q(r) = \frac{4\pi r^2 k_w}{d_w}(T_i^w - T_o^w) = \frac{4\pi r^2 k_w}{d_w}\Delta T_w \quad (10)$$

where k_w is thermal conductivity of the steel pipe wall, W/m/K; d_w is thickness of pipe wall, m; T_o^w is temperature of the outer pipe wall, K; and ΔT_w is the temperature drop due to heat conduction through the pipe wall, K.

One can write the overall temperature difference between the surface of the droplet and the outer pipeline wall as:

$$T_i^g - T_o^w = \Delta T_c + \Delta T_i + \Delta T_d + \Delta T_w \quad (11)$$

By substituting the various ΔT from Equations (7) through (10) into Equation (11), the amount of heat transferred through a droplet of radius r can be expressed as:

$$q(r) = \frac{T_i^g\left(1 - \dfrac{2\sigma}{H_{fg}r\rho}\right) - T_o^w}{\dfrac{r}{4\pi r^2 k_{H_2O}} + \dfrac{1}{2\pi r^2 h_i} + \dfrac{d_w}{4\pi r^2 k_w}} \quad (12)$$

The total heat flux for a unit area of the pipe wall covered by a large number of droplets of various sizes can be calculated by summing all the fluxes, which can be written as:[14]

$$Q = \int_{r_{min}}^{r_{max}} q(r)N(r)dr \quad (13)$$

where r_{max} is maximum radii of droplet, m, and r_{min} is minimum radii of droplet, m.

There are two flux equations, (6) and (13), and three unknowns, Q, T_i^g, and $\dot{m}$. Writing the mass balance closes the system and enables the calculation of the condensation rate for dropwise condensation.

Mass Balance

All the water condensing at the pipe wall comes from the gas phase, i.e., the water vapor needs to pass through the mass-transfer boundary layer to get to the wall. Therefore, one can equate the condensation rate to the mass flux of water through the gas phase. When noncondensable gases are present, the resistance to mass transfer of water vapor in the boundary layer can be rather significant. This makes the heat and mass transfer coupled and, therefore, they have to be solved simultaneously. One can write:

$$\dot{m} = \rho_g \beta_g (x_b^g - x_i^g) \tag{14}$$

where β_g is the mass-transfer coefficient in the gas boundary layer, m/s; x_b^g is the mass fraction of water vapor in the bulk gas flow, kg_v/kg_g; x_i^g is the mass fraction of water vapor at the gas-liquid interface, kg_v/kg_g; and ρ_g is density of gas, kg_g/m^3.

The mass-transfer coefficient for the gas boundary layer can be estimated using the analogy[18] between heat and mass transfer, according to:

$$\rho_g \beta_g = \frac{h_g}{\hat{C}_p} Le^{-2/3} \tag{15}$$

where $Le = k_g/r_g \hat{C}_p D_v$ is the Lewis number and D_v is the diffusivity of water vapor in the gas phase, m^2/s.

The mass fraction of water vapor in a saturated gas mixture x(T) is a function of temperature T and can be calculated according to:

$$x(T) = \frac{p_{sat}(T) M_{H_2O}}{p_{tot} M_{gas}} \tag{16}$$

where $p_{sat}(T)$ is the saturation vapor pressure as a function of temperature, kPa; p_{tot} is total pressure, kPa; M_{H_2O} is the molecular weight of water; and M_{gas} is the mean molecular weight of gas.

Therefore, this constitutes another way that the heat and mass-transfer processes are coupled:

$$x_b^g = x(T_b^g) = \frac{p_{sat}(T_b^g) M_{H_2O}}{p_{tot} M_{gas}} \tag{17}$$

$$x_i^g = x(T_i^g) = \frac{p_{sat}(T_i^g) M_{H_2O}}{p_{tot} M_{gas}} \tag{18}$$

To be able to solve the set of coupled heat and mass Equations (6), (13), and (14) and obtain the condensation rate, one needs to know the minimum and maximum size of the droplets that are found on a condensing steel surface.

Determination of Minimum and Maximum Radii of Droplets

Minimum radius[14] — The saturation temperature and pressure in equilibrium are slightly dependent on the shape of the interface between the gas and the liquid. The difference of saturation temperature between the curved surface and the flat surface is thought of as the minimum driving force (i.e., subcooling temperature) to form a droplet on the solid surface. Using the Clapyron relation and the equation of equilibrium on the curved surface, the minimum droplets can be calculated for a given wall subcooling through:

$$r_{min} = \frac{2 T_s \sigma}{H_{fg} \rho \Delta T} \tag{19}$$

Maximum radius — It is well known that gas velocity has a great influence on TLC. On one hand, it affects the heat and mass transfer in the gas boundary layer (Equations [3] and [14]), which are some of the most important steps in the whole condensation process. On the other hand, the drag force exerted by the flowing gas onto the droplets is the key factor for determining droplet size and motion at the top of the line. Through an analysis of the forces acting on a suspended droplet, it is possible to gain some insight into the mechanics of droplet growth and motion. In Figure 3, forces are considered as acting on a single hemispherical suspended droplet at the top of the line.

—The drag force, F_D^x, represents the pull by the flowing gas exerted on the droplet. It can be expressed by:[19]

$$F_D^x = \frac{1}{2} C_D \ \rho_g \ A \ v_g^2 \tag{20}$$

where C_D is the drag coefficient; $A = r^2\pi/2$ is the frontal area of a hemispherical droplet, m^2; and v_g is gas velocity, m/s.

The drag coefficient, C_D, depends on the shape of the droplet. For a sphere, the C_D is dependent on the Reynolds number and varies from 0.07 to 0.5. However, in the range of Reynolds numbers typical for TLC, the $C_D = 0.44$.

—The "friction" force F_f^x represents the adhesion between droplet and the steel wall that opposes the drag force and keeps the droplet in place. For a suspended droplet, an empirical equation is adopted from Bikerman:[20]

$$F_f^x = k_f \times \sigma \times r \tag{21}$$

where σ is the surface tension, N/m, and k_f is the friction coefficient, which is a function of inner pipe

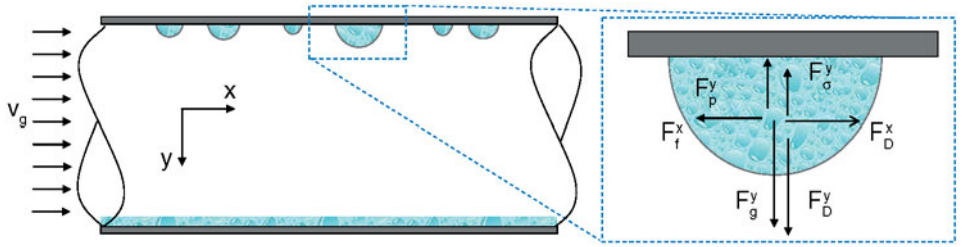

FIGURE 3. *Force analysis on a single droplet. F_B^y: buoyancy; F_σ^y: surface tension force; F_g^y: gravity force; F_D^y: flow drag force in y direction; F_f^x: friction force between the liquid droplet and the solid wall; F_D^x: flow drag force in x direction; V_g: gas velocity.*

surface roughness, h:

$$k_f = f(h) \tag{22}$$

Bikerman[21] performed a series of experiments on the surface of steel to determine the effect of surface roughness on the sliding droplets. It was found that when h is less than 0.5 μm the coefficient k_f changes significantly with roughness. But, when h is in the range from 0.5 μm to 3.0 μm, the coefficient k_f is approximately constant around 1.5.

—Gravity force F_g^y tends to either detach the droplet from the top of the pipe or cause it to slide down the sides of the pipe:

$$F_g^y = \rho \frac{4}{6} \pi r^3 g \tag{23}$$

—The downward drag force F_D^y arises due to the hemispherical shape of the droplets. No explicit expressions for calculation of this force have been found. In this study it is assumed:

$$F_D^y = \frac{1}{2} F_D^x \tag{24}$$

—The surface tension force F_σ^y keeps the droplet attached to the pipe wall and counters the effect of gravity. For a hemispherical droplet it can be calculated as:[22]

$$F_\sigma^y = \pi r^2 \frac{2\sigma}{r} \tag{25}$$

—The buoyancy F_B^y for a suspended hemispherical droplet can be calculated as:

$$F_B^y = \frac{4}{6} \pi r^3 \rho_g \tag{26}$$

where ρ_g is gas density, kg/m^3.

Very small droplets are firmly attached to the steel surface, i.e., the friction force is much larger than the drag force, $F_f^x > F_D^x$, and the droplet cannot slide along the pipe wall. Also, the surface tension and the pressure forces exceed the gravity and downward drag forces, $F_\sigma^y + F_B^y > F_g^y + F_D^y$, so the droplet does not detach and fall. Clearly, all the forces are a function of the droplet diameter. As condensation proceeds and a droplet grows, the effect of gravity increases fastest (with r^3). When the droplet reaches a critical size, a force balance in either x direction or y direction is reached. If the force balance in y direction is established before that in x direction, the droplet will fall down before it slides away. If the force balance in x direction is established before that in y direction, the droplet will slide along the pipe before it detaches and falls down. In either case, this represents the lifetime of a single droplet, and the maximum radius r_{max} of the droplet can be calculated.

Verification of the Condensation Model

With the model described above, the condensation rate for a dropwise regime can be calculated for a wide range of experimental conditions. To verify the model, some experiments have been performed in large-scale, high-temperature, high-pressure flow loops. The test section (Figure 4) where the data were collected was equipped with a cooling system, which is used to control the inner wall temperature through the adjustment of flow rate of cooling water. When hot wet gas flow contacts the cooler inner wall, condensation happens and the condensed water is drained to the liquid collector on the downstream. If the condensation rate for the whole inner surface of the text section is assumed to be uniform, it can be calculated (total volume of liquid divided by surface area and time) in mL/m^2/s. The parameters and their ranges are listed in Table 1. The comparison between experiments and model prediction are shown in Figure 5. The condensation model gives a good prediction of condensation rate.

In a separate series of experiments,[23] an in situ video camera was inserted into the test section (Figure 4) in one probe port at the bottom of the line to record the information about the lifetime of droplets, motion of droplets, and the maximum size of droplets at different conditions. In the model development, it is found that gas temperature, gas velocity, and gas

pressure are the most important factors for determining the maximum size and motion of droplets. In the experiments, the effect of all these major parameters was investigated. In various experiments, all parameters except gas velocity were kept constant and the maximum size of droplets then was measured as a function of the gas velocity. The measured maximum size of droplet is compared with the predictions in Figure 6 and very good agreement is achieved. Note how, under the given set of conditions, the droplet lifetime ends due to dislodgement by gravity at low velocities while at high velocity this happens as a result of gas drag force.

CORROSION MODEL

It is well known that the dropwise condensation is a random process. From a statistical point of view, every point on the metal surface has the same probability to be covered by a certain size of droplets at any given time. Therefore, the condensation rate can be assumed uniform over the entire surface. Although one point can corrode more than another at the beginning of the process, the entire surface will be corroded uniformly after some time. This way, the calculations can be carried out as if the surface was covered by a uniform liquid layer, which follows continuous cycles of growth and detachment (just like a single droplet).

To make it feasible, one needs to simplify the mathematical challenge in describing a complex random corrosion process occurring under a family of growing hemispherical droplets with a known-size distribution. Following the argument presented above, a family of two-dimensional hemispherical droplets is represented with a one-dimensional liquid layer of liquid (as shown in Figure 7). Droplet/layer growth due to condensation is represented by the increase in the height of the water column until the maximum size of the droplet, r_{max}, is reached. At that point, the droplet

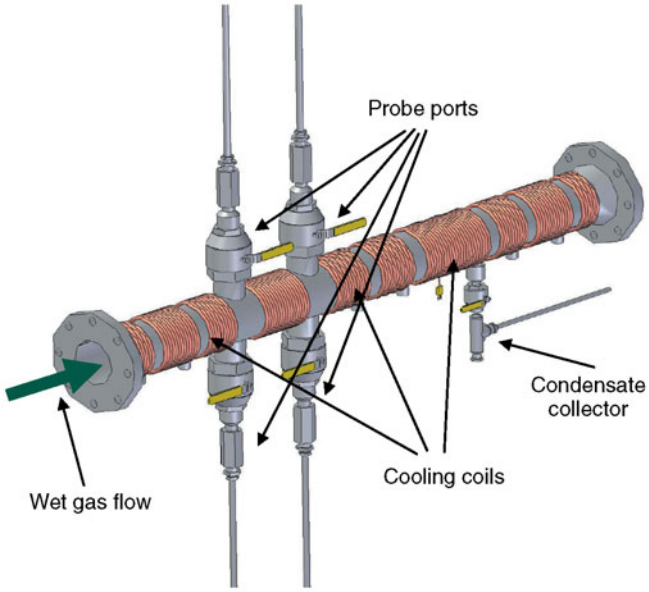

FIGURE 4. *Schematic of the test section in the flow loop.*

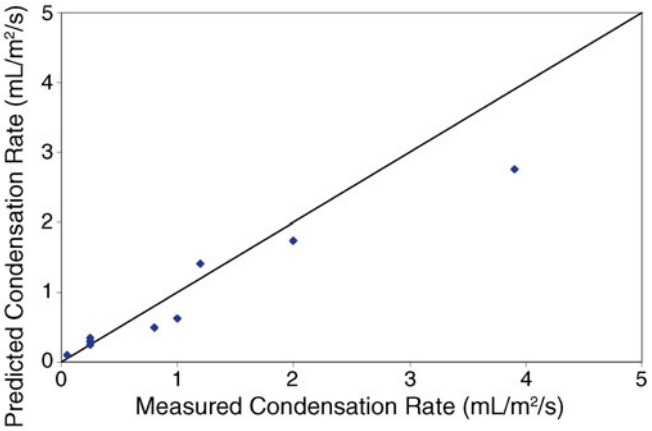

FIGURE 5. *Comparison of measured and predicted condensation rates.*

TABLE 1
Test Conditions in Large Scale Loop

	Range	
	Minimum	**Maximum**
Variable Parameters		
Absolute pressure (bar)	3	8
p_{CO_2} (bar)	0.13	8
Gas temperature (°C)	40	90
Condensation rate (mL/m²/s)	0.05	1
Gas velocity (m/s)	5	15
Free HAc concentration in the tank (ppm)	0	1,000
Constant Parameters		
Steel type	API X65	
Liquid phase composition	Deionized water	
Test duration (weeks)	3	
Internal diameter of pipe (in.)	4	

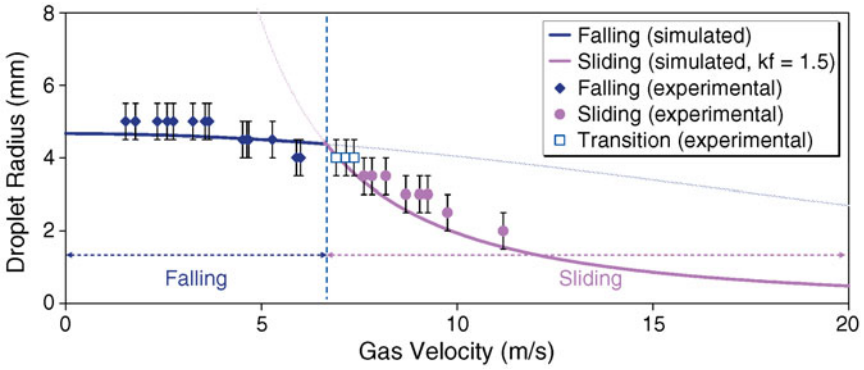

FIGURE 6. *The transition between sliding droplets and falling droplets (T_g = 25°C, P_T = 1 bar, k_f =1.5).*

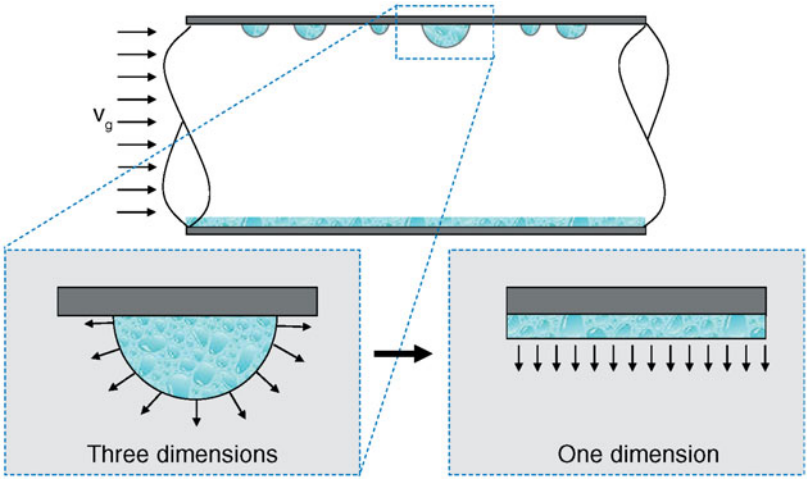

FIGURE 7. *The simplification from a three-dimensional problem to a one-dimensional problem.*

is dislodged and a new droplet starts growing in its place; this is simulated by reducing the size of the water column to minimum size of the droplet, r_{min}, and the cycle starts all over again.

The corrosion at the top of the line (or anywhere else for that matter) involves three important processes occurring simultaneously:

—chemical reactions, including homogeneous (dissociation, dissolution, etc.) and heterogeneous (precipitation of corrosion product scales)
—electrochemical reactions at the metal surface
—transport of species in the liquid droplet

Since these processes occur at different rates, the slowest one will be the rate controlling process, which will determine the corrosion behavior. These processes are modeled according to the physics underlying the different phenomena. Fundamental equations, already published by Nešić and coworkers,[9-11] are used to quantify the whole process mathematically. All constants in the equation system, such as equilibrium constants, reaction rate constants, and diffusion coefficients, are taken from the open literature referenced in Nešić's papers.[9-11]

Chemical reactions

Water dissociation	$H_2O \Leftrightarrow H^+ + OH^-$
Dissolution of carbon dioxide	CO_2 (g) $\Leftrightarrow CO_2$ (aq)
Carbon dioxide hydration	$CO_2 + H_2O \Leftrightarrow H_2CO_3$
Carbonic acid dissociation	$H_2CO_3 \Leftrightarrow H^+ + HCO_3^-$
Bicarbonate anion dissociation	$HCO_3^- \Leftrightarrow H^+ + CO_3^{2-}$
Acetic acid liquid/vapor equilibrium	HAc (aq) $\Leftrightarrow$ HAc (vap)
Acetic acid dissociation	$HAc \Leftrightarrow H^+ + Ac^-$

All the reactions shown above can be in equilibrium if the reaction rates are fast compared to other processes in the corroding system. According to stoichiometry, the reaction rate for species j can be calculated in the k-th chemical reaction:

$$R_j = a_{jk}\Re_k, \quad j = 1,2,\ldots n_s; \quad k = 1,2,\ldots n_r \qquad (27)$$

where tensor notation applies for the subscripts, a_{jk} is the stoichiometric matrix ($n_s \times n_r$ size) where row j represents the j-th species, column k represents the k-th chemical reaction, $\Re_k$ is the reaction rate vector, n_s is the number of species, and n_r is the number of reactions.

Transport Processes[9]

In the droplets, the transport of species can be described using a species conservation equation. The expression for the transport of species j in the presence of chemical reactions is valid for the pure liquid in the droplet as well as for the liquid in the porous surface scale:

$$\frac{\partial \varepsilon C_j}{\partial t} = -\frac{\partial(\kappa N_j)}{\partial y} + \varepsilon R_j \quad (28)$$

where C_j is the concentration of species j, moles/m^3; ε and κ are volumetric porosity and surface permeability of the scale, respectively (both equal to outside the corrosion product layer); N_j is the flux of species j, moles/m^2·s; R_j is the source or sink of species j due to chemical reaction, moles/m^3·s; t is time, s; and y is the spatial coordinate.

The transport of species has three components: diffusion, convection, and electromigration. In the first approximation, it can be assumed that the liquid in the droplets is stagnant, and therefore, no convection term exists in the species conservation equation. The electromigration is neglected as well and the electroneutrality equation is used instead:

$$\sum_j z_j \times C_j = 0 \quad (29)$$

where z_j is the number of charge for species j.

Therefore, the flux contains only a diffusion term and can be expressed using Fick's law:

$$N_j = -D_j \times \frac{\partial C_j}{\partial y} \quad (30)$$

where D_j is the molecular diffusivity of species j, m^2/s.

Combining all equations above, the overall species conservation equation in the droplet becomes:

$$\frac{\partial \varepsilon C_j}{\partial t} = D_j \frac{\partial^2(\kappa C_j)}{\partial y^2} + \varepsilon R_j \quad (31)$$

The permeability κ of surface scales is a function of porosity and tortuosity of the film. An empirical correlation $\kappa = \varepsilon^{1.5}$ from Nešić, et al.,[9] can be adopted to calculate the permeability.

Scale Growth

The calculation of the porosity ε and the overall scale growth model is taken entirely from Nešić and Lee.[11] For $FeCO_3$, there is an additional species conservation equation written in the same form as for other species (with the diffusion term neglected as $FeCO_3$ is a solid):

$$\frac{\partial C_{FeCO_3}}{\partial t} = R_{FeCO_3} \quad (32)$$

The volumetric porosity ε describes the morphology of the $FeCO_3$ scales and is the principal scale parameter affecting the transport of species:

$$\varepsilon = \frac{V_{void}}{V_{total}} = \frac{(V_{total} - V_{FeCO_3})}{V_{total}} = 1 - \frac{C_{FeCO_3} \times M_{FeCO_3}}{\rho_{FeCO_3}} \quad (33)$$

where M_{FeCO_3} is $FeCO_3$ molecular weight (115.8 kg/mol) and ρ_{FeCO_3} is $FeCO_3$ density (3.9 kg/m^3).

The scale growth Equation (32) can then be expressed as a function of porosity:

$$\frac{\partial \varepsilon}{\partial t} = -\frac{M_{FeCO_3}}{\rho_{FeCO_3}} R_{FeCO_3} \quad (34)$$

The $FeCO_3$ precipitation/dissolution reaction is modeled using van Hunnik's equation:[24]

$$R_{FeCO_3} = \frac{A}{V} \times e^{52.4 - \frac{119.8}{RT}} \times K_{sp} \times (S-1) \times (1 - S^{-1}) \quad (35)$$

where K_{sp} is the solubility product for $FeCO_3$ (moles/m^3)^2 and S is supersaturation ($S = \frac{C_{Fe^{2+}} \times C_{CO_3^{2-}}}{K_{sp}}$).

The surface-to-volume ratio, A/V, for the porous scale is calculated locally throughout the porous scale as:

$$\frac{A}{V} = \frac{\varepsilon^2 \times (1-\varepsilon)}{\Delta x} \quad (36)$$

where Δx is the characteristic size of an $FeCO_3$ crystal, m.

Initial and Boundary Conditions

Initial Conditions — Uniform concentrations of species as determined by chemical equilibria are used as initial conditions for all species.

Boundary Conditions — On the outer boundary of the droplet, which is in contact with the gas, the boundary conditions are different for different species. For "volatile" species including CO_2, HAc, and H_2S, the concentrations (C_j) are held constant as calculated by Henry's law:

$$C_j = H_j \rho_j \quad (37)$$

where H_j is the Henry's law constant for species j and ρ_j is the partial pressure of species j in gas phase, kPa.

For other species found only in the liquid phase, a zero flux boundary condition is imposed at the droplet outer boundary.

At the metal surface, zero flux is specified for the species not involved in the electrochemical reactions. A number of electrochemical reactions are happening at the metal surface:

Cathodic reactions:

Hydrogen reduction	$2\ H^+ + 2\ e^- \rightarrow H_2$
Direct reduction of carbonic acid	$2\ H_2CO_3 + 2\ e^- \rightarrow H_2 + 2\ HCO_3^-$
Water reduction	$2\ H_2O + 2\ e^- \rightarrow H_2 + 2\ OH^-$

Anodic reactions:

Electrochemical dissolution of iron $Fe \rightarrow Fe^{2+} + 2\ e^-$

If the species j is not a participant in an electrochemical reaction, the flux is zero ($N_j = 0$) at the metal surface. On the other hand, the flux for species involved in the electrochemical equation can be calculated through:

$$N_j = -\frac{i_j}{n_j F} \tag{38}$$

where i_j is the partial current for species j, A/m^2, and n_j is the number of moles of electrons exchanged per mole of species j.

From the Volmer-Butler equation, the correlation between the current density i and potential E for a cathodic/anodic reaction involving species j can be expressed as:

$$i_j = \pm\, i_{0,j} \times 10^{\pm\frac{E-E_{rev,j}}{b_j}} \tag{39}$$

where $i_{0,j}$ is the exchange current density, A/m^2, $E_{rev,j}$ is reversible potential, V, and b_j is the Tafel slope, V.

In a spontaneous corrosion process, the open-circuit potential E (also called corrosion potential) is the same for all involved cathodic and anodic reactions. Therefore, it can be calculated through the charge conservation equation below:

$$\sum_1^{na} i_j^a = \sum_1^{nc} i_j^c \tag{40}$$

where n_a and n_c are the total number of anodic and cathodic reactions, respectively.

Numerical Methods

Since all equations are strongly and nonlinearly coupled through the chemical reaction term, they have to be solved simultaneously, together with the boundary conditions and initial conditions. The species conservation equations and the scale growth equation are discretized using a finite difference method and a nonuniform grid. A fully implicit time discretization scheme is used here for reasons of stability, and all nonlinear terms are linearized in variable space.

Most of the equations and techniques described above for the corrosion model are the same as proposed originally by Nordsveen, et al.[10] However, the domain of calculation had to be adapted to the TLC scenario to take into account the growth and demise of droplets with time.

The growth of the droplet is simulated by controlling (moving) the position of the liquid/vapor interface, i.e., the outer boundary of the droplet. In reality, when the droplet reaches its maximum size and is removed from the top of the line, some liquid remains. This is even more true in the presence of porous corrosion product scales, which hold water in the pores much like a sponge. This effect is included in the model. At the very beginning of the calculation when a first droplet with a minimum radius is generated, the initial concentrations in the droplet are set by equilibria for pure, freshly condensed water. When this droplet grows, the outer boundary of the computational domain is extended. When the droplet detaches, the computational domain is shrunk back to match the initial (minimum) droplet size while the concentrations of species in that small droplet are unchanged from what they were before detachment. The same is true if there is a corrosion scale; the species concentrations in the porous scale are retained after droplet detachment. The new, freshly condensed droplet starts its lifetime on the outer side of the existing scale, i.e., the computational domain has the initial thickness equal to thickness of scale plus minimum droplet size.

Verification of Corrosion Model

From Figure 8, which shows a typical simulation result at specific conditions, it can be seen that the corrosion rate at the very beginning is very high because the fresh condensation water is very corrosive. The corrosion rate, however, decreases dramatically as the protective scale forms on the metal surface in the first day. As the scale grows and becomes denser, the corrosion rate is further decreased and remains at a very low "steady-state" value in long exposure. The jagged appearance of the corrosion rate curve is due to the many droplets that form, grow, and detach during simulation, each "fluctuation" representing a single droplet's lifetime. When a new, freshly condensed droplet forms, the corrosion rate increases temporarily and then rapidly decreases as the droplet saturates with $FeCO_3$, leading to a pH increase.

In most TLC cases, the general corrosion rate is expected to decrease rapidly to a very small value, since the chemistry in the droplets is ideal for the formation of protective corrosion product scale (small liquid volume, large corrosion rate leading to rapid $FeCO_3$ supersaturation). From Figure 9 it follows that even at a low gas temperature (40°C), the formation of the corrosion scale still retards the corrosion rate dramatically. In the simulation, it is found that both the concentration of iron ions and pH are always very high. For example, at these conditions (Figure 9), the pH in fresh condensed water is pH 3.8, which is also the boundary condition at the interface of the droplets. But, at the metal surface, the iron ion concentration builds up due to corrosion and can be as high as

600 ppm (w/w). As a result of the corrosion process, the pH increases and rapidly reaches pH 6.3, which leads to rapid protective film formation.

From the comparison between the experimental data and simulation results (Figures 8 and 9), it is seen that the model can accurately predict the trend of corrosion rate with time. Although the model overpredicts the corrosion rate for short-term experiments (2 days), it gives a reasonable prediction for long-term experiments. The discrepancy for short-term experiments probably results from the introduced approximation of a 2D problem in a 1D approach.

Several large-scale flow loops have been built at the Institute for Corrosion and Multiphase Technology (Athens, Ohio) to try to simulate as closely as possible the real field conditions. The description of these loops and the results are given elsewhere.[23,25] The parameters, which are covered in the experiments discussed below, are shown in Table 1. In these experiments, after the system at the set conditions reaches the equilibrium, weight-loss coupons are mounted on the probe, which are inserted into the test section through the probe ports. All the experiments were conducted over long periods of time, up to 3 weeks, with weight-loss coupons collected during the 2nd, 7th, 14th, and 21st day of exposure. The influence of several parameters including gas temperature, gas velocity, CO_2 partial pressure, condensation rate, and HAc concentration were investigated. The comparison between experimental data and predicted results in Figure 10 show a satisfactory agreement. In the simulation the model slightly overpredicts the corrosion rates for short-term experiments (2 days), which makes some points in this graph deviate from the diagonal line.

CONCLUSIONS

❖ A mechanistic model has been developed, which includes dropwise condensation, gas liquid equilibria, and corrosion process descriptions. This model takes into account the most important parameters in CO_2 TLC: gas temperature, CO_2 partial pressure, gas velocity, condensation rate, and HAc concentration. All these effects are described by mathematical equations, which are based firmly on the physics behind the processes involved. The model can predict the dropwise condensation rate and the evolvement of the uniform corrosion rate with time.

❖ Through comparisons with long-term experiments, the model shows reasonable performance in the prediction of general corrosion rate at the top of the line.

ACKNOWLEDGMENTS

Research for this project is supported by BP, ConocoPhillips, ENI, and Total. The authors acknowledge these companies for their technical and financial support and the permission to present the results.

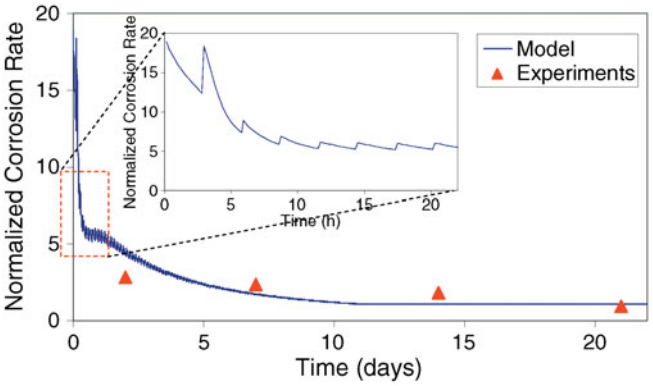

FIGURE 8. *The comparison between the model and long-term experiments (T_g = 70°C, V_g = 5 m/s, P_T = 3 bar, p_{CO_2} = 2 bar, condensation rate = 0.25 mL/m²/s).*

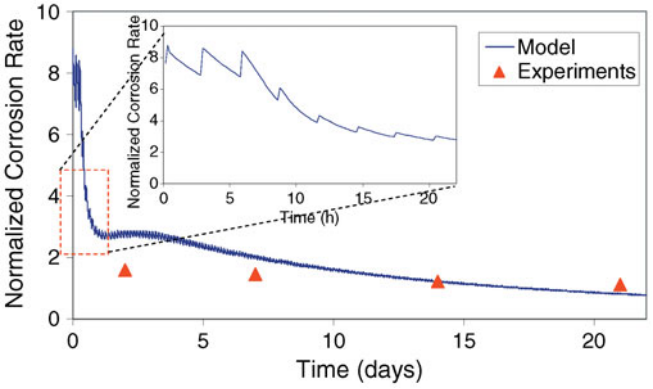

FIGURE 9. *The comparison between the model and long-term experiments (T_g = 40°C, V_g = 5 m/s, P_T = 3 bar, p_{CO_2} = 2 bar, condensation rate = 0.25 mL/m²/s).*

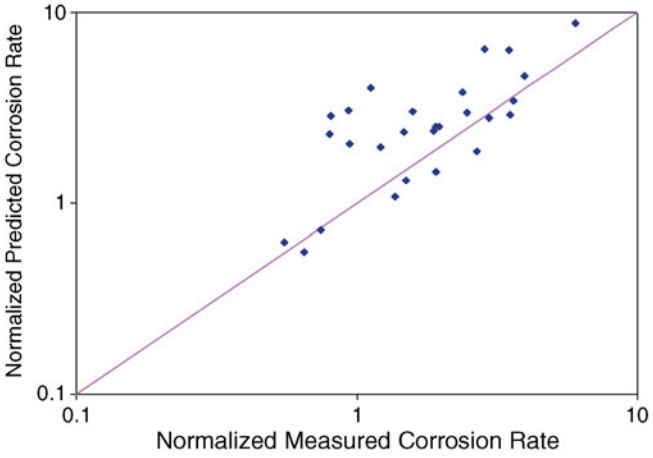

FIGURE 10. *The comparison between experimental data and predicted results.*

REFERENCES

1. M. Estavoyer, "Corrosion Problems at Lack Sour Gas Field," in H_2S Corrosion in Oil and Gas Production" (Houston, TX: NACE International, 1981), p. 905.

2. S. Olsen, A. Dugstad, "Corrosion Under Dewing Conditions," CORROSION/91, paper no. 472 (Houston, TX: NACE, 1991).
3. C. de Waard, U. Lotz, "Prediction of CO_2 Corrosion of Carbon Steel," CORROSION/93, paper no. 69 (Houston, TX: NACE, 1993).
4. Y.M. Gunaltun, D. Supriyatamam, J. Achmad, "Top-of-the-Line Corrosion in Multiphase Gas Lines: A Case History," CORROSION/99, paper no. 36 (Houston, TX: NACE, 1999).
5. Y.M. Gunaltun, D. Larrey, "Correlation of Cases of Top-of-Line Corrosion with Calculated Water Condensation Rates," CORROSION/2000, paper no. 71 (Houston, TX: NACE, 2000).
6. B.F.M. Pots, E.L.J.A. Hendriksen, "CO_2 Corrosion Under Scaling Conditions the Special Case of Top-of-the-Line Corrosion in Wet Gas Pipelines," CORROSION/2000, paper no. 31 (Houston, TX: NACE, 2000).
7. F. Vitse, S. Nešić, Y. Gunaltun, "Semi-Empirical Model for Prediction of the Top-of-the-Line Corrosion Risk," CORROSION/2002, paper no. 02245 (Houston, TX: NACE, 2002).
8. F. Vitse, S. Nešić, Y. Gunaltun, Corrosion 59 (2003): p. 1,075-1,084.
9. S. Nešić, J. Postlethwaite, S. Olsen, Corrosion 52 (1996): p. 280-294.
10. M. Nordsveen, S. Nešić, R. Nyborg, Corrosion 59 (2003): p. 443-456.
11. S. Nešić, K.L.J. Lee, Corrosion 59 (2003): p. 616-628.
12. Y. Utaka, A. Saito, Int. J. Heat Mass Transf. 31 (1988): p. 1,113-1,120.
13. J.W. Rose, L.R. Glicksman, Int. J. Heat Mass Transf. 16 (1973): p. 411-425.
14. J.W. Rose, Int. Commun. Heat Mass Transf. 15 (1988): p. 449-473.
15. M. Abu-Orabi, Int. J. Heat Mass Transf. 41 (1998): p. 81-87.
16. C. Graham, P. Griffith, Int. J. Heat Mass Transf. 16 (1973): p. 337-346.
17. F.W. Dittus, L.M.K. Boetler, Public Engineering 2 (1930): p. 443-447.
18. K. Stephan, Heat Transfer in Condensation and Boiling (New York, NY: Springer-Verlag, 1992), p. 84.
19. F.M. White, Fluid Mechanics, 4th ed. (Boston, MA: McGraw-Hill International, 1999), p. 460.
20. J.J. Bikerman, J. Colloid Sci. 5 (1950): p. 349-359.
21. J.J. Bikerman, Physical Surfaces (New York, NY: Academic Press, 1970), p. 278.
22. A.W. Adamson, Physical Chemistry of Surfaces (New York, NY: John Wiley and Sons, 1990), p. 21.
23. M. Singer, B. Brown, Z. Zhang, A. Camacho, D. Hinkson, S. Nešić, "Top-of-the-Line Corrosion Joint Industry Project," TLC Board Meeting Report at Institute for Corrosion and Multiphase Technology, Ohio University, 2006.
24. E.W.J. van Hunnik, B.F.M. Pots, E.L.J.A. Hendriken, "The Formation of Protective $FeCO_3$ Corrosion Product Layer in CO_2 Corrosion," CORROSION/96, paper no. 6 (Houston, TX: NACE, 1996).
25. C. Mendez, M. Singer, A. Camacho, S. Hernandez, S. Nešić, Y. Gunaltun, M. Joosten, Y. Sun, P. Gabetta, "Effect of Acetic Acid, pH, and MEG on the CO_2 Top-of-the-Line Corrosion," CORROSION/2005, paper no. 05278 (Houston, TX: NACE, 2005).